Efficiency and loss mechanisms of plasmonic Luminescent Solar Concentrators

Clemens Tummeltshammer, Mark S. Brown, Alaric Taylor, Anthony J. Kenyon and Ioannis Papakonstantinou*

Department of Electronic and Electrical Engineering, University College London London WC1E 7JE, United Kingdom

*i.papakonstantinou@ucl.ac.uk

Abstract: Using a hybrid nanoscale/macroscale model, we simulate the efficiency of a luminescent solar concentrator (LSC) which employs silver nanoparticles to enhance the dye absorption and scatter the incoming light. We show that the normalized optical efficiency can be increased from 10.4% for a single dye LSC to 32.6% for a plasmonic LSC with silver spheres immersed inside a thin dye layer. Most of the efficiency enhancement is due to scattering of the particles and not due to dye absorption/re-emission.

OCIS codes: (050.1755) Computational electromagnetic methods; (080.0080) Geometric optics; (220.1770) Concentrators; (250.5403) Plasmonics; (350.6050) Solar energy.

References and links

1. W. H. Weber and J. Lambe, "Luminescent greenhouse collector for solar radiation," Appl. Opt. **15**, 2299–2300 (1976).
2. A. Goetzberger and W. Greube, "Solar energy conversion with fluorescent collectors," Appl. Phys. **14**, 123–139 (1977).
3. W. G. J. H. M. van Sark, K. W. J. Barnham, L. H. Slooff, A. J. Chatten, A. Büchtemann, A. Meyer, S. J. McCormack, R. Koole, D. J. Farrell, R. Bose, E. E. Bende, A. R. Burgers, T. Budel, J. Quilitz, M. Kennedy, T. Meyer, C. D. M. Donegá, A. Meijerink, and D. Vanmaekelbergh, "Luminescent solar concentrators–a review of recent results," Opt. Express **16**, 21773–21792 (2008).
4. V. Sholin, J. D. Olson, and S. A. Carter, "Semiconducting polymers and quantum dots in luminescent solar concentrators for solar energy harvesting," J. Appl. Phys. **101**, 123114 (2007).
5. M. G. Debije, P. P. C. Verbunt, B. C. Rowan, B. S. Richards, and T. L. Hoeks, "Measured surface loss from luminescent solar concentrator waveguides," Appl. Opt. **47**, 6763–6768 (2008).
6. R. Reisfeld, "New developments in luminescence for solar energy utilization," Opt. Mater. **32**, 850–856 (2010).
7. S. Chandra, J. Doran, S. J. McCormack, M. Kennedy, and A. J. Chatten, "Enhanced quantum dot emission for luminescent solar concentrators using plasmonic interaction," Sol. Energ. Mat. Sol. Cells **98**, 385–390 (2012).
8. H. R. Wilson, "Fluorescent dyes interacting with small silver particles; a system extending the spectral range of fluorescent solar concentrators," Sol. Energ. Mat. **16**, 223–234 (1987).
9. S. Agostinelli, "Geant4—a simulation toolkit," Nucl. Instrum. Methods Phys. Res., Sect. A: Accelerators, Spectrometers, Detectors and Associated Equipment **506**, 250–303 (2003).
10. P. Bharadwaj, P. Anger, and L. Novotny, "Nanoplasmonic enhancement of single-molecule fluorescence," Nanotechnology **18**, 044017 (2007).
11. S. Kühn, U. Håkanson, L. Rogobete, and V. Sandoghdar, "Enhancement of single-molecule fluorescence using a gold nanoparticle as an optical nanoantenna," Phys. Rev. Lett. **97**, 017402 (2006).
12. X. Miao, I. Brener, and T. S. Luk, "Nanocomposite plasmonic fluorescence emitters with core/shell configurations," J. Opt. Soc. Am. B **27**, 1561–1570 (2010).
13. K. R. Catchpole and A. Polman, "Design principles for particle plasmon enhanced solar cells," Appl. Phys. Lett. **93**, 191113 (2008).
14. J. S. Batchelder, A. H. Zewail, and T. Cole, "Luminescent solar concentrators. 2: Experimental and theoretical analysis of their possible efficiencies," Appl. Opt. **20**, 3733–3754 (1981).

#191121 - $15.00 USD Received 24 May 2013; revised 21 Jun 2013; accepted 28 Jun 2013; published 8 Jul 2013

15. E. D. Palik, Handbook of Optical Constants of Solids (Academic, 1985).
16. E. A. Coronado and G. C. Schatz, "Surface plasmon broadening for arbitrary shape nanoparticles: A geometrical probability approach," J. Chem. Phys. **119**, 3926–3934 (2003).
17. C. F. Bohren and D. R. Huffman, *Absorption and scattering of light by small particles* (Wiley, 1983).
18. E. M. Purcell, "Spontaneous emission probabilities at radio frequencies," Phys. Rev. **69**, 681 (1946).
19. P. Bharadwaj and L. Novotny, "Spectral dependence of single molecule fluorescence enhancement," Opt. Express **15**, 14266–14274 (2007).
20. L. Novotny and B. Hecht, *Principles of Nano-Optics* (Cambridge University, 2006).
21. Oregon Medical Laser Center, "Rhodamine B," http://omlc.ogi.edu/spectra/PhotochemCAD/html/009.html (2013).
22. M. Fikry, M. M. Omar, and L. Z. Ismail, "Effect of host medium on the fluorescence emission intensity of rhodamine B in liquid and solid phase," J. Fluoresc. **19**, 741–746 (2009).
23. A. V. Deshpande and E. B. Namdas, "Correlation between lasing and photophysical performance of dyes in polymethylmethacrylate," J. Lumin. **91**, 25–31 (2000).
24. National Renewable Energy Laboratory, "Reference solar spectral irradiance: Air mass 1.5," http://rredc.nrel.gov/solar/spectra/am1.5/ (2013).
25. F. L. Arbeloa, P. R. Ojeda, and I. L. Arbeloa, "Fluorescence self-quenching of the molecular forms of rhodamine B in aqueous and ethanolic solutions," J. Lumin. **44**, 105–112 (1989).
26. C. V. Bindhu, S. S. Harilal, G. K. Varier, R. C. Issac, V. P. N. Nampoori, and C. P. G. Vallabhan, "Measurement of the absolute fluorescence quantum yield of rhodamine B solution using a dual-beam thermal lens technique," J. Phys. D: Appl. Phys. **29** 1074–1079 (1996).
27. E. Yablonovitch, "Statistical ray optics," J. Opt. Soc. Am. **72**, 899–907 (1982).
28. H. A. Atwater and A. Polman, "Plasmonics for improved photovoltaic devices," Nat. Mater. **9**, 205–213 (2010).

1. Introduction

Luminescent solar concentrators (LSCs), which concentrate sunlight without having to track the sun, offer a promising means to reduce the costs of solar energy. The first LSCs were proposed in the late 70s [1–3]; however, limited efficiencies and dropping fossil fuel prices in the 80s caused interest in LSCs to fade. The recent surge in renewable energy generation and the availability of new technologies have brought LSCs back into the spotlight.

However, current LSC designs suffer from low efficiency, which causes them to be uneconomic. The main loss mechanisms are 1) *Re-absorption losses:* re-emitted light could be absorbed by another fluorophore, since absorption and emission spectra of the fluorophore generally overlap increasing the risk of thermal dissipation; 2) *Escape cone losses:* the re-emission of photons is generally isotropic due to random dye orientation and hence a portion of these photons will be emitted within the escape cone and leave the LSC. Escape cone losses become even more dominant due to successive re-absorption occurrences; 3) *Limited spectral efficiency:* the absorption band of fluorophores is often too narrow to make use of the entire solar spectrum.

Reducing these loss mechanisms improves the LSC's optical efficiency, which is the ratio between the number of photons reaching a solar cell and the number of photons incident on the top surface. Reported optical efficiencies and the importance of the different loss mechanisms of LSCs vary considerably depending on factors such as the dye molecule used, its concentration, the LSC size and the wavelength band of interest. For example in [4] the optical efficiencies ranged from 1.6% to 19.8% for various fluorophores. These authors modeled a $25 \times 76 \times 5\,\mathrm{mm}^3$ LSC and showed that for CdSe/ZnS quantum dots with low quantum yield of 50%, about 43.9% of light is dissipated as heat. Increasing the quantum efficiency resulted in strong escape cone losses with an estimated loss of 78% for a $40 \times 5 \times 0.5\,\mathrm{cm}^3$ LSC [3]. These results are consistent with experimental measurements in [5], which showed that for a $50 \times 50 \times 3\,\mathrm{mm}^3$ LSC doped with Lumogen F Red305, escape cone losses were also dominant with approximately 40 to 50% of photons being lost through the top and bottom surfaces.

It has been proposed to combine the field of plasmonics with LSCs to overcome the mentioned losses [6–8]. Placing a thin dye doped layer atop a thick undoped layer is expected to strongly reduce re-absorption losses, and thereby escape cone losses. The reduced absorp-

#191121 - $15.00 USD Received 24 May 2013; revised 21 Jun 2013; accepted 28 Jun 2013; published 8 Jul 2013

tion efficiency of the thinner active layer is intended to be mitigated by introducing a layer of metallic nanoparticles. The illuminated metallic nanoparticles induce local surface plasmon resonances, resulting in (a) strong near-field enhancements that will excite the fluorophore due to dipole-dipole interactions and (b) scattering of the arriving light so that some photons are totally internally reflected at the top and bottom surfaces of the LSC. In [6] Reisfeld suggested to use silver nanoparticles to enhance the efficiency of LSCs. Chandra et al. [7] investigated a mixture of gold nanoparticles and CdSe/ZnS core-shell quantum dots and showed a fluorescence enhancement of up to 53%. Wilson [8] suggested to use small silver particles to enhance the fluorescence of dye molecules absorbing in the near infrared, as they suffer from low quantum yields. However, no publication showed optical efficiency results for the entire plasmonic LSC device. Also, there is no information for the extent to which the enhanced absorption and the scattering would contribute to the efficiency of the LSC. The aims of this work are to investigate the optical efficiency and potential of a plasmonic LSC for the first time, to differentiate between photons being picked up by a solar cell due to scattering and dye absorption/re-emission, and to determine the plasmonic LSC's limitations by examining its loss channels.

We have developed a hybrid model that enables the simulation of a plasmonic LSC device for various configurations. The hybrid model combines the finite-difference time-domain (FDTD) method as a nanoscale modeling tool (although other methods such as finite element method could be used as well), an interface developed in MATLAB and Monte-Carlo ray tracing (Geant4 [9]) as a macroscopic modeling tool. We investigate three different plasmonic LSC configurations, which are shown in Fig. 1. In the first configuration, silver spheres are immersed within a thin dye layer that is placed within an undoped waveguide. There is a 3 nm thin undoped spacing between the spherical nanoparticles and the dye molecules to prevent most of the dye absorbed photons from being quenched. A sphere is chosen due to its simplicity and its common use [10, 11]. The second configuration is similar to the first, but the silver spheres are now replaced by spherical shells that additionally have dye molecules within a PMMA core. It was shown in [12] that very strong fluorescent enhancements can be achieved within a silver shell. In the third configuration, silver discs are placed atop the waveguide. Discs are chosen since they are very effective at scattering light into the waveguide, as was shown for solar cells [13]. For all three configurations the nanoparticles are distributed randomly atop or within the dye layer.

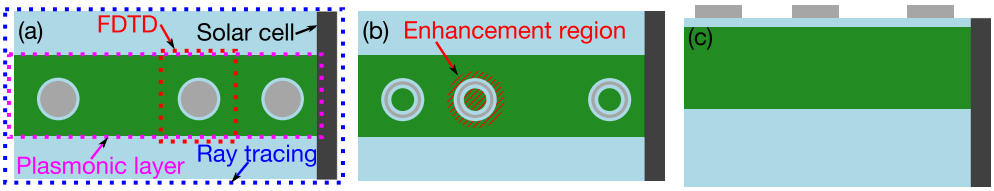

Fig. 1. (a) Sphere, (b) shell and (c) disc configurations. Blue, green and silver represent undoped PMMA, dye doped PMMA and the nanoparticles, respectively. While the thicknesses of the waveguide and the dye layer look similar in the Figs., they are orders of magnitude different in the simulations (200 nm dye layer vs. 5 mm waveguide). (a) Shows the hybrid model setup. A single nanoparticle is simulated on the nanoscale using FDTD. MATLAB determines the behavior of the entire plasmonic layer. Ray tracing then simulates the whole LSC treating the plasmonic layer as an interface. (b) Shows the enhancement region for one single shell.

We use silver as the nanoparticle material, since it was shown to be more effective in enhancing the fluorescence of nearby dye molecules than other noble metals such as gold and aluminum [10]. Rhodamine B is chosen as a prototype dye molecule, since it is a commonly uti-

#191121 - $15.00 USD Received 24 May 2013; revised 21 Jun 2013; accepted 28 Jun 2013; published 8 Jul 2013

lized fluorophore in LSC studies [4, 14]. The dipole moments of the dye molecules are oriented arbitrarily within the PMMA. However, it should be noted that our hybrid model is general enough to allow any material/dye molecule combination and any non-random dipole moment orientation.

In Section 2 our hybrid model is presented, Section 3 discusses the ray tracing results of the investigated LSC designs, and the paper is concluded in Section 4.

2. Hybrid Model

The working principle of the hybrid model is depicted in Fig. 1(a) for the spherical configuration. The hybrid model allows us to feed the results of a time consuming nanoscale simulation, such as the interaction of light with nanoparticles, into ray tracing, which benefits from simplicity and high speed. The approach is to translate FDTD results, such as cross sections, into interaction probabilities for the plasmonic layer used in ray tracing. A photon that reaches the plasmonic layer (see Fig. 2) is either (a) absorbed or (b) scattered by a nanoparticle, (c, d) absorbed by a dye molecule, or (e) no interaction takes place. If the photon is dye absorbed, it is either (c) quenched or (d) re-emitted at a longer wavelength. The following Sections 2.1-2.3 illustrate how to calculate the probabilities of each event. We present the FDTD simulations in Section 2.1, the linkage between the FDTD outputs and the inputs to ray tracing developed in MATLAB in Section 2.2, and a new boundary process we added to the ray tracing algorithm (Geant4) to accommodate the various inputs in Section 2.3.

In our work we assume that the nanoparticles are isolated from each other and randomly distributed, but, with appropriate modifications, periodic or interacting structures such as optical nanoantennas could be modeled as well. These modifications would include using Bloch boundary conditions for the FDTD plane wave simulations and incorporating a discrete angular spectrum in the far field instead of a continuous angular spectrum. The use of this tool is not limited to LSCs, but can be used for other optical systems such as plasmonic solar cells or liquid crystal displays.

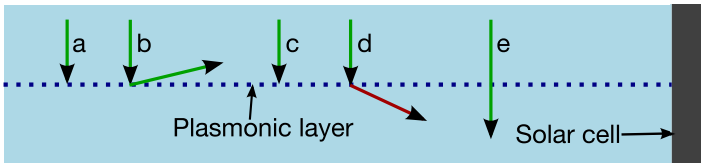

Fig. 2. Setup for ray tracing and various photon paths. (a) Absorbed by a nanoparticle (b) Scattered by a nanoparticle (c) Dye absorbed and then quenched (d) Dye absorbed and re-emitted at different wavelength (e) No interaction with the nanoparticles or the dye molecules.

2.1. FDTD

Here we investigate the behavior of light near the nanoparticles shown in Fig. 1 using FDTD. The system response to a plane wave and a dipole are computed. A plane wave source yields the absorption and differential scattering cross sections and field enhancements around the nanoparticles, while an electric dipole source allows us to simulate the near-field interactions between dyes and nanoparticles. Both are broadband sources ranging from 300 nm to 800 nm, as this range covers all the cross section, electric field, and dye molecule absorption and emission peaks. To derive the plane wave response of the system to unpolarized light, which is the polarization of sunlight, one has to incoherently average the results of two orthogonal polarizations.

#191121 - $15.00 USD Received 24 May 2013; revised 21 Jun 2013; accepted 28 Jun 2013; published 8 Jul 2013

The dielectric constant of silver is based on the values reported by Palik [15]. For the shell configuration the thickness of the silver is smaller than the conduction electron mean free path of the bulk material. We use a classical approach as described in [16] to account for the size dependent dielectric constant, which hardly changes the real dielectric constant, but increases the imaginary part particularly for higher wavelengths. Furthermore the computational cell is surrounded by Perfectly Matched Layers imitating a single, isolated object. We use a maximum mesh step size of 1 nm for the nanoparticle and 5 nm for other regions of interest such as the monitors, since the field gradient is large around the nanoparticles. The refractive index of the LSC is set to 1.5, a value that very well approximates the refractive index of PMMA, the most commonly used host material, over the chosen frequency space.

The metallic structures are simulated with radii of 30, 50 and 70 nm. For the shell the inner radii are equal to 24, 40 and 56 nm respectively, while the height of the discs is kept constant at 30 nm. No results for smaller or bigger radii are shown, as the optical efficiency results start to worsen for radii smaller than 50 nm and the results for spheres above 50 nm are similar since the overall shape of the cross section changes only slightly (see Section 3).

Nanoparticle cross sections and field enhancements

The absorption σ_{abs} and differential scattering $\frac{\mathrm{d}\sigma_{\text{sca}}}{\mathrm{d}\Omega}$ cross sections are given by [17]

$$\sigma_{\text{abs}}(\lambda,\chi) = \frac{P_{\text{abs}}(\lambda,\chi)}{I(\lambda,\chi)} \qquad \frac{\mathrm{d}\sigma_{\text{sca}}}{\mathrm{d}\Omega}(\theta,\phi,\lambda,\chi) = \frac{P_{\text{sca}}(\theta,\phi,\lambda,\chi)}{I(\lambda,\chi)} \tag{1}$$

where P_{abs}, P_{sca}, I, λ and χ represent the power absorbed by the particle, the power scattered by the particle per unit solid angle, the intensity of the incoming plane wave, the wavelength and the incoming angle respectively. The spherical coordinates, denoted by the inclination angle θ and the azimuthal angle ϕ, indicate the direction of the scattered light $\mathbf{n}$. Since the spheres and shells sit within a homogeneous environment and benefit from spherical symmetry, the cross sections are independent of χ. As this is not true for the discs, we simulate discs for varying χ.

Figure 3(a) shows the cross sections expressed in efficiencies (the simulated cross section divided by the cross-sectional area of the nanoparticle [17]) for all three configurations with a radius of 50 nm. It is preferential to have a small absorption cross section to limit Ohmic losses and a high scattering cross section, as some of the scattered light's wave vector will have a large enough angle with the normal to the PMMA/air interface for total internal reflection to occur. Hence the sphere configuration looks the most promising, since the scattering cross section peak is about three times as large as the absorption cross section peak and also spans across a wide wavelength band. Similarly, the disc configuration benefits from a three times larger scattering cross section, while the shell's scattering cross section is only slightly larger.

In addition to high absorption and scattering cross sections, very strong field enhancements occur around a silver nanoparticle. The electric field intensity enhancement EF and its spatial average $\overline{\text{EF}}$ are given by

$$\text{EF}(\mathbf{x},\lambda) := \frac{|\mathbf{E}_{\text{total}}|^2}{|\mathbf{E}_0|^2}(\mathbf{x},\lambda) = \frac{|\mathbf{E}_0+\mathbf{E}_{\text{sca}}|^2}{|\mathbf{E}_0|^2}(\mathbf{x},\lambda) \qquad \overline{\text{EF}}(\lambda) = \frac{1}{V}\int_V \text{EF}(\mathbf{x},\lambda)\mathrm{d}\mathbf{V} \tag{2}$$

where $\mathbf{E}_0$ is the incoming electric field, $\mathbf{E}_{\text{sca}}$ is the electric field due to the scattering of the particle and V is the volume of interest.

Since the electric field intensity enhancement is different to unity only just around a nanoparticle, we term the volume of dyes in the proximity of the nanoparticles as the *enhancement region* (see Fig. 1(b)). The extent of the enhancement region is chosen such that the field enhancement outside of it is close to unity. Consequently the enhancement region volumes are equal to 1.52, 1.73 and 0.74 million nm^3 for the 50 nm sphere, shell and disc respectively.

#191121 - $15.00 USD Received 24 May 2013; revised 21 Jun 2013; accepted 28 Jun 2013; published 8 Jul 2013

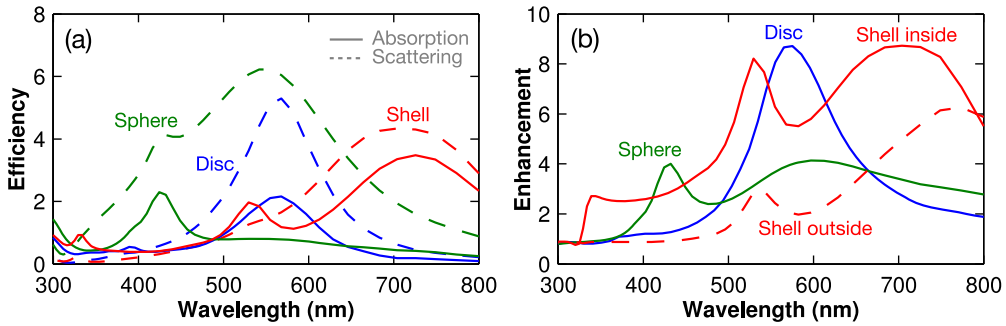

Fig. 3. Plane wave response to the sphere (green), disc (blue) and shell (red) configurations with a radius of 50 nm. (a) Absorption (solid) and scattering (dashed) cross sections. (b) Mean electric field intensity enhancement within the enhancement region. The red solid line represents the volume inside the silver shell and the red dashed line the volume outside of the shell.

The resulting average electric field intensity enhancement within the enhancement region for all three configurations with a radius of 50 nm is shown in Fig. 3(b). The disc configuration and the volume inside the shell experience the strongest average enhancement of 8.7, while the sphere configuration reaches an enhancement of 4.1. Since the enhancement region is also the largest for the shell, the shell's dye absorption enhancement is expected to be the most pronounced.

Figure 4(a) shows the various angles describing the incoming plane wave and the far field. The plasmonic layer is assumed to be along the $x-y$ plane. As an illustration, Fig. 4(b) shows the differential scattering cross section, Eq. (1), for the 50 nm sphere. The wavelength is equal to 541 nm (the scattering peak) and the incoming angle χ (the angle between the wave vector $\mathbf{k}$ and the plasmonic layer normal) is equal to 0° . The results are shown for unpolarized light.

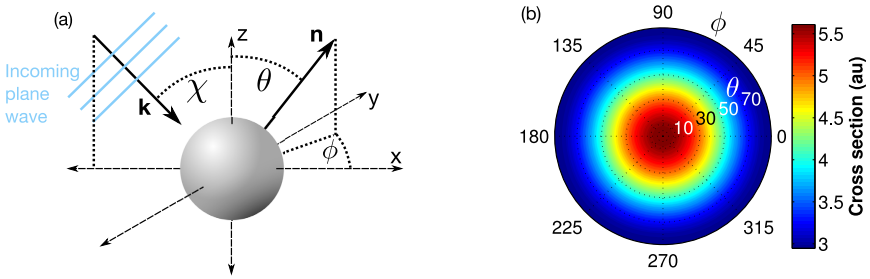

Fig. 4. (a) Notation used to describe the incoming plane wave and the far field information. The plasmonic layer is along the $x-y$ plane. The incoming plane wave vector $\mathbf{k}$ and the plasmonic layer normal are at an angle χ. The far field direction vector $\mathbf{n}$ is described by the inclination angle θ and the azimuthal angle ϕ. (b) The differential scattering cross section for the 50 nm sphere with χ and λ equal to 0° and 541 nm and θ ranging from 0° to 90°.

Quantum yield

It was predicted by Purcell that the emission rate of an emitter such as a molecule is also dependent on the molecule's environment [18]. The dipole simulations allow us to investigate which share of the dye absorbed power will be radiated to the far field and in which direction.

#191121 - $15.00 USD Received 24 May 2013; revised 21 Jun 2013; accepted 28 Jun 2013; published 8 Jul 2013

The share radiated to the far field is denoted as the quantum yield and can be written as [19]

$$q = \frac{\gamma_{\mathrm{rad}}/\gamma_{\mathrm{rad}}^0}{\gamma_{\mathrm{rad}}/\gamma_{\mathrm{rad}}^0 + \gamma_{\mathrm{abs}}/\gamma_{\mathrm{rad}}^0 + (1-q^0)/q^0} \tag{3}$$

with γ_{rad}, γ_{abs} and the superscript denoting the radiative and non-radiative decay rates and the respective parameter in free space. The non-radiative decay rate γ_{abs} is due to the environment and would be equal to zero in free space. In the case of a silver nanoparticle, γ_{abs} is due to the energy transfer from the molecule to the nanoparticle and the resulting Ohmic losses.

By normalizing with respect to the radiated power by a dipole in a homogeneous environment P_{rad}^0, the classical theory, and thus the FDTD results, can be compared with quantum theory through the radiative and non-radiative enhancement factors $M_{\mathrm{rad}} := \gamma_{\mathrm{rad}}/\gamma_{\mathrm{rad}}^0 = P_{\mathrm{rad}}/P_{\mathrm{rad}}^0$ and $M_{\mathrm{abs}} := \gamma_{\mathrm{abs}}/\gamma_{\mathrm{rad}}^0 = P_{\mathrm{abs}}/P_{\mathrm{rad}}^0$ [20], where P_{rad} and P_{abs} represent the power radiated to the far field and the power absorbed by the nanoparticle respectively. In the dipole case the probability that a photon of wavelength λ emitted by a dye at the simulated position will radiate to the far field at angles θ (inclination) and ϕ (azimuthal) is given by

$$\Pr(\mathrm{DYE}(\theta,\phi)|\lambda) = \frac{P_{\mathrm{rad}}(\theta,\phi|\lambda)/P_{\mathrm{rad}}^0(\lambda)}{P_{\mathrm{rad}}(\lambda)/P_{\mathrm{rad}}^0(\lambda) + P_{\mathrm{abs}}(\lambda)/P_{\mathrm{rad}}^0(\lambda) + (1-q^0)/q^0} \tag{4}$$

Since a random dipole/dye orientation is assumed in our model, the system response to any arbitrary dipole orientation has to be averaged. It can be shown that for radiative and non-radiative enhancements this mean is equivalent to the average of three orthogonal orientations which yields the quantum yield for arbitrary dye orientation

$$q^{\mathrm{av}} = \frac{(M_{\mathrm{rad}}^{p_x}+M_{\mathrm{rad}}^{p_y}+M_{\mathrm{rad}}^{p_z})/3}{(M_{\mathrm{rad}}^{p_x}+M_{\mathrm{rad}}^{p_y}+M_{\mathrm{rad}}^{p_z})/3 + (M_{\mathrm{abs}}^{p_x}+M_{\mathrm{abs}}^{p_y}+M_{\mathrm{abs}}^{p_z})/3 + (1-q^0)/q^0} \tag{5}$$

where $M_{\mathrm{rad}}^{p_x}$ is equal to the radiative enhancement due to a dipole in the x-direction and likewise for y and z. Figure 5 shows the average quantum yield depending on the distance between the sphere's surface and the dye. The intrinsic quantum yield q^0 is equal to 80%. Between 300 and 420 nm quenching dominates and most of the dye absorbed energy is lost to heat. However, for longer wavelengths more than 70% is radiated to the far field starting at a distance of 15 nm and thus quenching is low.

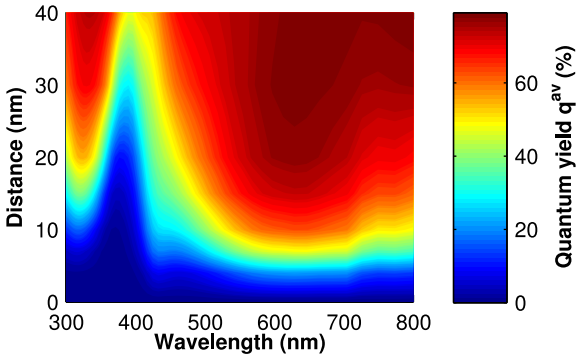

Fig. 5. Average quantum yield q^{av} as a function of wavelength and distance from the 50 nm sphere with an intrinsic quantum yield q^0 of 80%.

#191121 - $15.00 USD Received 24 May 2013; revised 21 Jun 2013; accepted 28 Jun 2013; published 8 Jul 2013

2.2. MATLAB interface

Here we introduce the process of translating the FDTD results of a single nanoparticle into interaction probabilities for the entire plasmonic layer used by ray tracing. First the nanoparticle interaction probabilities are calculated, then the probability that a photon is absorbed by a dye is computed, and finally the spatial probability distribution of dye absorption is presented.

Nanoparticle absorption and scattering probability

To derive the interaction probabilities necessary for ray tracing, one has to multiply cross sections with the nanoparticle concentration per unit area C_{NP} at the interface. For a given wavelength λ and incoming angle χ, the probabilities of a photon being absorbed or scattered in a direction defined by the spherical angles θ and ϕ (see Fig. 4(a)) by a nanoparticle are equal to

$$\Pr(\mathrm{NP}_{\mathrm{abs}}|\lambda,\chi) = C_{\mathrm{NP}}\sigma_{\mathrm{abs}}(\lambda,\chi) \qquad \Pr(\mathrm{NP}_{\mathrm{sca}}(\theta,\phi)|\lambda,\chi) = C_{\mathrm{NP}}\frac{\mathrm{d}\sigma_{\mathrm{sca}}}{\mathrm{d}\Omega}(\theta,\phi,\lambda,\chi) \quad (6)$$

The nanoparticle concentration C_{NP} must be chosen so that the assumption of negligible interaction between the nanoparticles is not violated, which means that the distance between them must be large enough so that cross sections do not overlap. While the total scattering cross section of the sphere or shell does not vary with incoming angle χ, the differential scattering cross section does. However no further FDTD simulation is needed; the differential scattering cross section for χ equal to 0° can just be rotated to derive the result for any other χ.

Dye absorption probability

The next task is to translate the properties of the dye, such as its molar concentration, and the FDTD results into a probability that the photon will be absorbed by the dye layer.

The environment not only strongly affects the decay channels of a fluorophore, as stated in Section 2.1, but can also enhance the excitation rate (rate of optical absorption). Since the dye molecules reside only within a very thin layer, we use the first approximation to Beer Lambert Law. The power absorbed by the arbitrarily oriented dyes in one infinitesimal volume element is given by [20]

$$\mathrm{d}P_{\mathrm{dye}}(\lambda) = \frac{1}{2}\sqrt{\frac{\varepsilon_0}{\mu_0}}n(\lambda)\sigma_{\mathrm{M}}(\lambda)c_D N_A|\mathbf{E}(\mathbf{x},\lambda)|^2\mathrm{d}\mathbf{V} \quad (7)$$

where ε_0, μ_0, n, σ_{M}, c_D and N_A denote the vacuum permittivity and permeability, refractive index, absorption cross section of a single dye molecule, molar dye concentration and Avogadro constant respectively. The model differentiates between the enhancement region of the nanoparticles and the remaining dye layer, since only in the enhancement region is the electric field altered due to the nanoparticles. Equation (7) is integrated over the enhancement region of one nanoparticle and then multiplied with the concentration of nanoparticles C_{NP}. Over the remaining dye layer, Eq. (7) is integrated assuming that the nanoparticles have no effect on the electric field there. For all three configurations we assume a dye layer thickness of 200 nm, as there is no considerable enhancement beyond this thickness for all simulated configurations and sizes.

The dye molecule absorption cross section σ_{M} in Eq. (7) and the emission spectrum are based on the data of Rhodamine B [21] (Fig. 6(a)), a typical organic dye. The goal of this work is to investigate and fairly compare various plasmonic LSC designs and not to examine different fluorophores. Thus we shift the peak absorption of the dye to the maximum electric field enhancement wavelength of the respective configuration. This will yield a maximum dye absorption and ensure that the results are independent of the peak enhancement wavelength. The peak emission wavelength is shifted accordingly to keep the Stokes shift constant at 22 nm. It was shown that the intrinsic quantum yield of Rhodamine B in PMMA is around 80% [22,23].

#191121 - $15.00 USD Received 24 May 2013; revised 21 Jun 2013; accepted 28 Jun 2013; published 8 Jul 2013

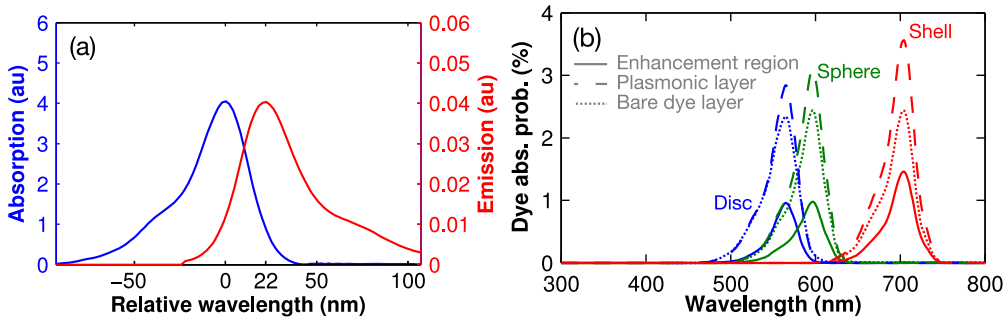

Fig. 6. (a) Absorption and emission spectra of Rhodamine B [21]. The *x*-axis is relative to the peak absorption wavelength. (b) Dye absorption probabilities for the 50 nm sphere (green), 50 nm disc (blue) and 50 nm shell (red). Solid lines represent the dye absorption probability in the enhancement region of the nanoparticles, dashed lines additionally consider the remaining dye layer (thus the entire plasmonic layer) and dotted lines the layer without nanoparticles. The dye molar concentration c_D is assumed to be 5×10^{-3} M.

Figure 6(b) shows the probability that a photon will be absorbed within the dye layer for a particle concentration C_{NP} of $12.73 \times 10^{12} m^{-2}$ (10% nanoparticle surface coverage) which ensures that most of the incoming light will interact either with the nanoparticles or the dye molecules. The solid lines show the probability that the photon is absorbed within the enhancement region of the nanoparticles, while the dashed lines additionally consider the remaining dye layer. The shell configuration dye absorbs the strongest in the enhancement region of the nanoparticles, since the average electric field enhancement $\overline{\mathrm{EF}}$ is the highest and the enhancement region volume is the largest out of the three configurations. In this configuration, about 41% of the photons absorbed by dye molecules will be absorbed in the enhancement region. The enhancement region accounts for only 11% of the total dye layer in this configuration. As a comparison the dotted lines show the dye absorption within the layer in the absence of any nanoparticles. The peak dye absorption increases from 2.4% for bare dye to 3.1% for the spherical nanoparticles corresponding to a 26.4% increase. Similarly, for the shell and disc configurations, the inclusion of the nanoparticles enhances the peak dye absorption by 46.2% and 21.4% respectively.

Position probability distribution of dye absorption

If a photon is absorbed by a dye molecule in the enhancement region of a nanoparticle, a probability distribution will determine where exactly the photon has been absorbed with respect to the nanoparticle. Since the absorption by the dye molecules is proportional to the electric field intensity at the location of the dye (see Eq. (7)) the probability distribution is a normalized version of the electric field intensity within the enhancement region of the nanoparticle. The locations for which a probability distribution is generated depends on where dipole simulation results are available.

Figure 7(a) shows the electric field intensity enhancement EF for a wavelength of 597 nm around the 50 nm sphere with the incoming plane wave vector parallel to the *z*-axis. Since the result is shown for unpolarized light, the enhancement is cylindrically symmetric. The resulting probability distribution for each simulated position is depicted in Fig. 7(b). The calculation considers that the position probabilities have a $\sin(\theta)$ and radial dependence where θ is the inclination angle.

#191121 - $15.00 USD Received 24 May 2013; revised 21 Jun 2013; accepted 28 Jun 2013; published 8 Jul 2013

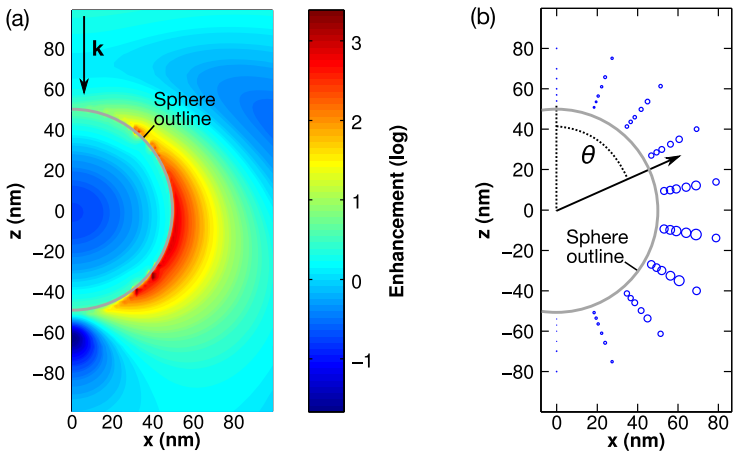

Fig. 7. For the 50 nm sphere and a wavelength of 597 nm: (a) Electric field intensity enhancement EF (log-scale). (b) Probability distribution for each position. The size of the rings represents the probability of a photon being absorbed at the respective position.

2.3. Geant4 boundary process

A boundary process is invoked in Geant4 once a photon reaches an interface (the materials on both sides can be the same though). In the case of the new boundary process developed for the plasmonic layer, the photon is either 1) absorbed by the nanoparticle, 2) scattered by the nanoparticle, 3) absorbed by a dye or 4) Fresnel reflected or refracted. The likelihood of each of these events occurring is dependent on the photon's wavelength and the incoming angle (ie $\Pr(\text{event}|\lambda,\chi)$). The probabilities mentioned above are given by Eq. (6) and the integral of Eq. (7). For each wavelength λ and incoming angle χ, one minus these probabilities determines the likelihood that the photon simply obeys the Fresnel equations.

In case a photon is absorbed by a dye molecule that is not in the enhancement region of a nanoparticle, a new wavelength will be drawn from the emission profile of the dye. The photon is then re-emitted isotropically with a quantum yield equal to the intrinsic quantum yield q^0. If averaged, the resulting emission profile of randomly oriented dichroic dye molecules within a finite but small volume is isotropic.

If the photon is dye absorbed in the enhancement region of a nanoparticle instead, a random location will be drawn from the position probability distribution described in Section 2.2. Given the position of absorption and a randomly chosen wavelength from the emission spectrum, the photon is either 1) quenched or 2) radiated at the new wavelength. The probability of quenching to occur is one minus the quantum efficiency of a randomly oriented dipole q^{av}, with q^{av} given by Eq. (5), while the differential radiation probability is given by Eq. (4).

The setup in ray tracing is shown in Fig. 2 with the new boundary (the plasmonic layer) being in the middle of the LSC for spheres and shells. For discs the interface would be on the top.

3. Results

Using ray tracing, the new boundary process and the MATLAB results, the optical efficiency of the plasmonic LSCs can be computed. First the three configurations for a radius of 50 nm are compared to a standard LSC. Then the optical efficiency's dependencies on the nanoparticle size, the intrinsic quantum yield and the LSC dimensions are investigated. Finally multiple plasmonic layers are simulated to examine a thicker layer.

The simulated LSC device has dimensions of $50 \times 50 \times 5\,\text{mm}^3$, unless stated otherwise,

#191121 - $15.00 USD Received 24 May 2013; revised 21 Jun 2013; accepted 28 Jun 2013; published 8 Jul 2013

which is in the range of commonly reported LSC sizes [3, 5]. All side facets are covered with solar cells. A source emits photons of different wavelengths impinging on the top surface at normal incidence and random positions. For each wavelength 50,000 photons are simulated to ensure that the optical efficiency results vary by less than 0.1%.

For the plasmonic LSCs either the top surface (disc configuration) or a surface in the middle of the LSC (shell and sphere configurations) are governed by our new boundary process described in Section 2.3. All the other interfaces are dictated by Fresnel theory. Since the aim of this work is to compare the different configurations, we neglect host absorption and assume that a photon enters a solar cell once it reaches one of the edge surfaces. This corresponds to the solar cells being index-matched.

3.1. LSC metric

A widely used metric for a LSC is the optical efficiency $\eta_{\mathrm{opt}}(\lambda)$, which is the ratio between the number of photons reaching the solar cells and the total number of photons incident on the top surface for each wavelength. The optical efficiency can be integrated and normalized with respect to the AM1.5 spectrum $A(\lambda)$ [24] to derive a wavelength independent figure of merit for the LSC.

$$\overline{\eta}_{\mathrm{opt}} = \frac{\int_{\lambda_1}^{\lambda_2} A(\lambda)\eta_{\mathrm{opt}}(\lambda)\mathrm{d}\lambda}{\int_{\lambda_1}^{\lambda_2} A(\lambda)\mathrm{d}\lambda} \tag{8}$$

where $\overline{\eta}_{\mathrm{opt}}$ denotes the AM1.5 normalized optical efficiency and $\lambda_1 = 300\,\mathrm{nm}$ and $\lambda_2 = 800\,\mathrm{nm}$ limit the wavelength range of interest as described in Section 2.1.

3.2. Plasmonic LSCs vs. bulk LSCs

Here we compare the normalized optical efficiencies for all three configurations with a radius of 50 nm to each other and to two non-plasmonic LSCs. One of the non-plasmonic LSCs consists of a PMMA waveguide that is entirely doped with dye molecules ("bulk") and the other one has a 200 nm thin layer of dye molecules (same thickness as plasmonic LSCs) within the undoped PMMA waveguide ("layer"). First the molar dye concentration c_D is fixed at $5 \times 10^{-3}\,\mathrm{M}$, a concentration used in a previous LSC study [4], and the particle concentration C_{NP} is varied to compare the plasmonic LSCs. Then the best performing plasmonic LSC is compared with the non-plasmonic LSCs while varying the molar dye concentration. For the plasmonic LSCs, the efficiency is shown as a function of nanoparticle surface coverage.

As shown in Fig. 8(a), the spherical configuration outperforms the other two configurations. The 50 nm sphere reaches a normalized efficiency of 21.3% at a coverage of 11.8%, while the shell's efficiency is equal to 7.8% at the same coverage. The disc configuration achieves an efficiency of 5.6% with a coverage of 9.4%. Increasing the particle concentration C_{NP} boosts the interaction probabilities and therefore improves the optical efficiency for all three configurations. However, starting at a particular particle concentration, the cross sections of neighboring nanoparticles start to overlap and cannot be considered as independent from each other anymore. Thus, there is a maximum coverage possible which differs between the configurations and sizes. The maximum nanoparticle surface coverage is around 12% for the 50 nm sphere and shell and around 10% for the 50 nm disc.

As the top performer, the 50 nm sphere is then compared to the "bulk" LSC in Fig. 8(b) as a function of dye concentration c_D using a nanoparticle surface coverage of 11.8%. The "bulk" LSC attains a maximum normalized optical efficiency of 10.4% at a concentration of $10^{-4}\,\mathrm{M}$. In comparison, the "layer" LSC only reaches an efficiency of 0.2% at $5 \times 10^{-3}\,\mathrm{M}$, since there is too little interaction with the incoming light. Interestingly, the efficiency of the 50 nm sphere configuration hardly changes as a function of dye concentration, which indicates that most of

#191121 - $15.00 USD Received 24 May 2013; revised 21 Jun 2013; accepted 28 Jun 2013; published 8 Jul 2013

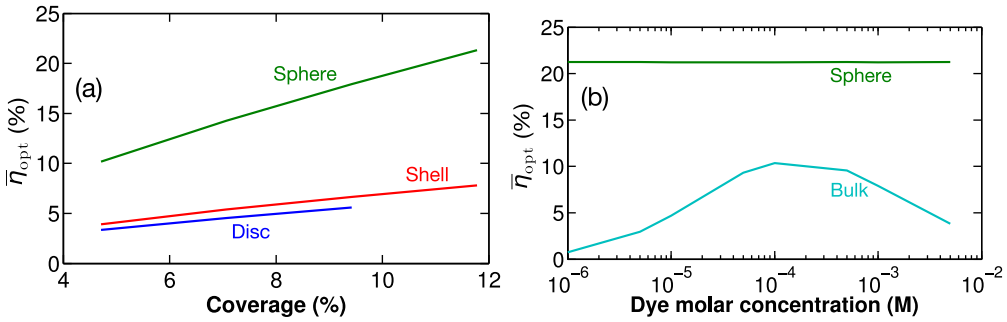

Fig. 8. (a) Normalised optical efficiencies for the sphere (green), disc (blue) and shell (red) configurations with 50 nm radius as a function of nanoparticle coverage (b) Normalised optical efficiencies for the sphere (green) and the "bulk" LSC (cyan) as a function of dye concentration.

the efficiency is due to scattering and not dye absorption/re-emission. Indeed at the highest dye concentration of 5×10^{-3} M, about 99.4% of all photons reaching an edge surface do so by scattering, which increases to 99.9% for 10^{-6} M. This mismatch is partly due to the spectrally narrow dye absorption profiles shown in Fig. 6(b). Furthermore, at the particle concentration $C_{\rm NP}$ used in the same Fig., the probabilities of being absorbed or scattered by the nanoparticle turn out to be much larger than the probability of being absorbed by the dye layer. For the 50 nm sphere the peak absorption and scattering probabilites are 23% and 62.2% respectively, while the dye absorption probability peak is equal to 3.1%.

To investigate the large efficiency differences between the plasmonic LSCs, Fig. 9 shows the fate of incident photons for the disc and the spherical configurations. Clearly the absorption by the nanoparticles closely follows the profile of the absorption cross sections in Fig. 3(a), while the share of photons reaching an edge surface matches the scattering cross sections. As mentioned above, the dye absorption suffers from being spectrally narrow and weak. For both the disc and sphere configurations, only around 4% of incident photons are dye absorbed at the respective peak wavelengths. One of the main reasons for the top performance of the spherical configuration is that the nanoparticle absorption and scattering peaks are more than 100 nm apart, while for the disc they occur at the same wavelength (see Fig. 3(a)). Also, the scattering cross section of the sphere is much wider than for the other configurations. Thus there is a wide wavelength band over which the spheres scatter very efficiently, but do not suffer as strongly from Ohmic losses. The discs and shells might scatter as efficiently at certain wavelengths, but a scattered photon generally impinges on the plasmonic surface multiple times before reaching the solar cell. If at the same wavelength the nanoparticle absorption cross section is also high, it is likely that the photon is lost to heat before it approaches the sides of the LSC.

The optical efficiency also strongly depends on the directionality of the scattering process. It is preferential for the scattered photon's direction to be outside of the escape cone, as the photon is then trapped within the waveguide through total internal reflection. In Fig. 9(c) the share that is scattered outside of the escape cone is compared for the three configurations. For the disc configuration, all the back-scattered light is lost as the discs sit atop the waveguide. As shown, the sphere and shell are more efficient than the disc at scattering outside of the escape cone.

3.3. Sphere configuration

The sphere is the top performer and scattering the main contributor to the optical efficiency. To investigate this further, the cross sections for varying radii are shown in Fig. 10(a). The smallest

#191121 - $15.00 USD Received 24 May 2013; revised 21 Jun 2013; accepted 28 Jun 2013; published 8 Jul 2013

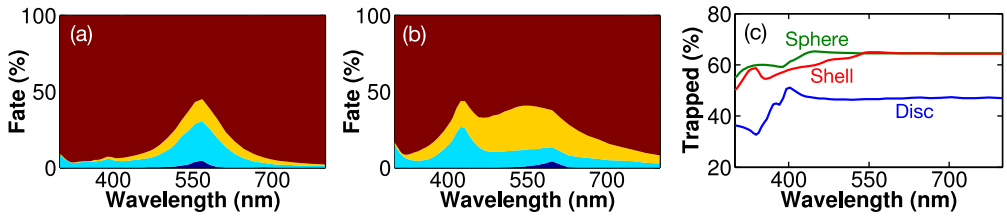

Fig. 9. Area plot for fate of incident photons for the (a) 50 nm disc and (b) 50 nm sphere configurations. Photons are either nanoparticle absorbed (light blue), dye absorbed (dark blue), picked up by the solar cell (yellow) or lost (dark red). (c) Trapping efficiency for 50 nm sphere (green), 50 nm disc (blue) and 50 nm shell (red) configurations at normal incidence.

sphere has distinct absorption and scattering peaks at the same wavelength of 467 nm, which causes its LSC efficiency to be worse than for the two larger sizes. Like the 50 nm sphere, the 70 nm sphere has its second scattering peak at a wavelength with small absorption cross section and a spectrally wide scattering cross section. Hence the normalized optical efficiencies of the two larger spheres are very similar. At a surface coverage of 7% the 30, 50 and 70 nm spheres attain a normalized optical efficiency of 8.1%, 14.1% and 14.9% respectively. Increasing the coverage for the 70 nm sphere to 12.3%, around the maximum possible coverage to avoid overlapping cross sections, yields an efficiency of 23.7%. Similar cross section shapes for larger spheres suggest that no further considerable improvement can be expected with increasing size.

To examine how the plasmonic LSC performs at larger sizes, the size of the top surface is gradually increased from the original dimensions of $50 \times 50\,\mathrm{mm}^2$ up to $1000 \times 1000\,\mathrm{mm}^2$. The results shown in Fig. 10(b) represent the "bulk" and the 70 nm sphere configurations as a function of geometrical gain which is equal to the top surface divided by the area of solar cells. The efficiency drops for both configurations as the photons have to cover a longer average distance to the solar cells. This increases the probability of successive interaction with the plasmonic layer or the dye molecules and thereby the probabilities of heat and escape cone losses. The results show that larger sizes seem to have a slightly stronger effect on the optical efficiency of the plasmonic LSC. Its normalized optical efficiency declines from 23.7% for the smallest size to 4.3% for the largest size (drop of 82%) while the "bulk" LSC decreases from 10.4% to 2.9% (drop of 72%). In contrast to the plasmonic LSC, the "bulk" LSC benefits from a Stokes shift, which reduces the risk of subsequent interactions.

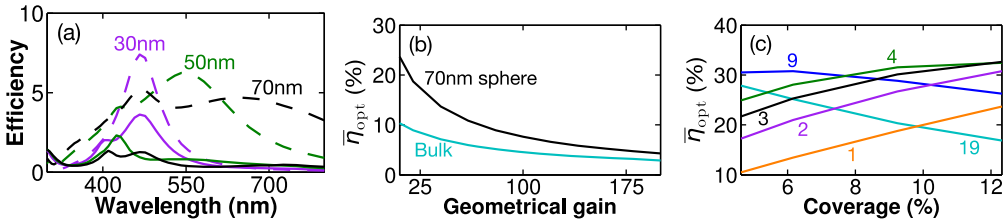

Fig. 10. (a) Absorption (solid) and scattering (dashed) cross sections of spheres with radii of 30 nm (purple), 50 nm (green) and 70 nm (black). (b) Optical efficiency as a function of geometrical gain for 70 nm sphere (black) and "bulk" LSC (cyan) (c) Optical efficiency for 1 (orange), 2 (purple), 3 (black), 4 (green), 9 (blue) and 19 (cyan) plasmonic layers.

It has been shown that at a high molar concentration c_D of 5×10^{-3} M, self quenching can occur and the quantum yield will be lower than the assumed 80% [25, 26]. Thus the effect of

#191121 - $15.00 USD Received 24 May 2013; revised 21 Jun 2013; accepted 28 Jun 2013; published 8 Jul 2013

a lower quantum yield on the 70 nm sphere configuration is investigated. Since for an intrinsic quantum yield q^0 of 80%, about 99% of the picked up photons reach the solar cells due to scattering and not dye absorption, little impact on the performance can be expected. Indeed the AM1.5 normalized optical efficiency drops by less than 1% while lowering the intrinsic quantum yield q^0 from 80% to 0%.

3.4. Multiple layers

So far the dye absorption has been quite low. Dye absorption could potentially be enhanced by using a volume distribution of plasmonic nanoparticles within the LSC. To emulate volume distributions of various thicknesses, we have stacked multiple plasmonic layers on top of each other. For these types of simulations, the previously presented FDTD/MATLAB calculations for the interaction probabilities are still valid. However, multiple plasmonic layers have now been included in the ray tracing simulation corresponding to a volume distribution of non-interacting nanoparticles. The normalized optical efficiencies shown in Fig. 10(c) are for plasmonic LSC devices using 70 nm spheres with 1, 2, 3, 4, 9, and 19 plasmonic layers for which the total dye layer thicknesses are equal to 200 nm, 400 nm, 600 nm, 800 nm, 1800 nm and 3800 nm respectively.

The addition of layers first improves the optical efficiency, since it has the same effect as increasing the particle concentration; it enhances the interaction probabilities. However at the same time the efficiency curves flatten out, as the optical efficiency gain from a higher coverage decreases with every supplementary layer. With 4 layers there is no longer a maximum normalized optical efficiency improvement for each additional layer. The maximum normalized optical efficiency of 32.6% is reached with 3 layers at a coverage of 12.3%. With 9 and 19 layers the optical efficiency even decreases with coverage, as Ohmic losses start to dominate due to the many layer crossovers a photon experiences.

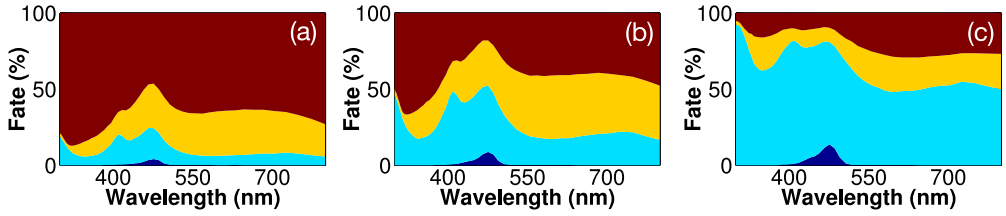

Fig. 11. Area plot for fate of incident photons which are either nanoparticle absorbed (light blue), dye absorbed (dark blue), picked up by the solar cell (yellow) or lost (dark red) for (a) 1, (b) 3 and (c) 19 plasmonic layers.

Figure 11 shows the fate of incident photons for the simulations with 1, 3 and 19 plasmonic layers and a coverage of 12.3%. Indeed the dye absorption share increases at the peak dye absorption wavelength of 476 nm from 4% for 1 layer to 8.7% and 13.7% for 3 and 19 layers respectively. Similarly the share of dye absorbed/re-emitted photons picked up by the solar cells with the incident photons having a wavelength of 476 nm increases from 5.2% to 8.6% and 15.4%. However the growth of dye absorption comes at the cost of higher Ohmic losses, with the AM1.5 normalized Ohmic losses surging from 11.1% to 28.4% and 62.4%.

4. Conclusion

We have shown that the AM1.5 normalized optical efficiency of a single dye $50 \times 50 \times 5\,\mathrm{mm}^3$ LSC device can be improved by 128.7% from 10.4% to 23.7% through the use of a single plasmonic layer. However, the enhancement does not derive from a balanced mixture of scattering

#191121 - $15.00 USD Received 24 May 2013; revised 21 Jun 2013; accepted 28 Jun 2013; published 8 Jul 2013

and dye absorption/re-emission but mostly from scattering. Furthermore spheres have proven to be much more efficient than shells and discs, since the absorption and scattering cross section peaks occur at different wavelengths for the 50 nm and 70 nm spheres. Also for these two configurations the scattering cross section stretches over a broad wavelength band ensuring that the nanoparticles interact with photons of varying wavelengths.

The normalized optical efficiency can be increased even further to 32.6% by using 3 plasmonic layers with a total thickness of 600 nm and a nanoparticle coverage of 12.3% in each layer, which is the optimum configuration we found. Multiple layers ensure more interaction with light including a stronger dye absorption yielding a higher optical efficiency of the device. Still scattering remains the main driver of the optical efficiency and if too many layers are included Ohmic losses start to dominate and worsen the efficiency of the LSC, with 62.4% photons lost to nanoparticle absorption for 19 layers.

It should be stressed that our results do not refute experimental results that indicate fluorescence enhancement in the presence of metallic nanoparticles [7, 10], but rather support them. As shown in Fig. 6(b), the nanoparticles enhance the absorption of the dye molecules and thus (depending on the quantum yield) also the fluorescence.

Since the dye absorption probability is about one order of magnitude smaller than the nanoparticle absorption probability, even a dye absorption enhancement of 46.2% for the shell configuration improves this mismatch only marginally. Thus the plasmonic LSCs would be almost as efficient without any dye layer, as the plasmonic layer mostly serves as a scatterer, which means the LSC performance is limited by the Yablonovitch limit [27]. In order to improve plasmonic LSCs, a more efficient interaction between nanoparticles and dye molecules over larger volumes has to be achieved. One potential solution is to excite surface plasmon polariton waves on a metallic structure at the back surface of the LSC. As the wave propagates along the surface, its evanescent tail will excite dye molecules in its vicinity. In this way energy can be transferred to the dyes efficiently, similar to what has been suggested for semiconductor solar cells [28].

Acknowledgments

This work was supported by the European Union Framework Programme 7 (FP7) via a Marie-Curie Career Integration Grant, Project No. 293567. We also acknowledge financial support from UCL BEAMS School via a PhD Impact Award.

#191121 - $15.00 USD Received 24 May 2013; revised 21 Jun 2013; accepted 28 Jun 2013; published 8 Jul 2013